Axion Dark Matter Search with Sensitivity near the Kim-Shifman-Vainshtein-Zakharov Benchmark Using the TM_{020} Mode

Sungjae Bae,[1,2,3,*] Junu Jeong,[2,4,*] Younggeun Kim,[2,5,6,*] SungWoo Youn,[1,2,†] Jinsu Kim,[1,2] Arjan F. van Loo,[7,8] Yasunobu Nakamura,[7,8] Seonjeong Oh,[1,2] Taehyeon Seong,[1,2] Sergey Uchaikin,[1,2] Jihn E. Kim,[9] and Yannis K. Semertzidis[2,3]

[1]*Dark Matter Axion Group, Institute for Basic Science, Daejeon 34126 Republic of Korea*
[2]*Center for Axion and Precision Physics Research, Institute for Basic Science, Daejeon 34051, Republic of Korea*
[3]*Department of Physics, Korea Advanced Institute of Science and Technology, Daejeon 34141, Republic of Korea*
[4]*Oskar Klein Centre, Department of Physics, Stockholm University, AlbaNova, SE-10691 Stockholm, Sweden*
[5]*Johannes Gutenberg-Universität Mainz, 55122 Mainz, Germany*
[6]*GSI Helmholtzzentrum für Schwerionenforschung GmbH, 64291 Darmstadt, Germany*
[7]*RIKEN Center for Quantum Computing, Wako, Saitama 351-0198, Japan*
[8]*Department of Applied Physics, Graduate School of Engineering, The University of Tokyo, Bunkyo-ku, Tokyo 113-8656, Japan*
[9]*Department of Physics, Seoul National University, Seoul 08826, Republic of Korea*

(Received 18 May 2025; accepted 1 August 2025; published 26 August 2025)

Axions, originally proposed to resolve the *CP* problem in the strong interaction, remain a leading dark matter candidate. While cavity haloscopes offer the most sensitive technique for detecting axions, searches have largely been limited to masses below 10 μeV. We report a sensitive search for axion dark matter with masses around 21 μeV, utilizing the TM_{020} mode of a cylindrical cavity equipped with an innovative tuning mechanism. Our search achieved a sensitivity of 1.7× the Kim-Shifman-Vainshtein-Zakharov benchmark over a 100-MHz range, representing a significant advance in this mass range. These results demonstrate that higher-order modes provide a viable strategy for extending haloscope searches into previously unexplored higher-mass regions.

DOI: 10.1103/f11t-qy8z

The nature of dark matter remains one of the greatest mysteries in modern science, and its discovery could provide deep insights into fundamental physics. Among the various candidates [1], the axion is particularly compelling, initially proposed to address the charge conjugation and parity symmetry problem in quantum chromodynamics. Predicted from the Peccei-Quinn mechanism through spontaneous breaking of global U(1) axial symmetry, the axion possesses well-defined properties [2]. The invisible models, Kim-Shifman-Vainshtein-Zakharov (KSVZ) [3,4] and Dine-Fischler-Srednicki-Zhitnitsky (DFSZ) [5,6], predict light, weakly interacting axions, suggesting they may have formed as cold, nonrelativistic particles in the early Universe and could significantly contribute to the observed dark matter density [7–9].

Over the past few decades, experimental efforts to detect axion signals have significantly progressed [10,11]. Haloscope experiments, which exploit the electromagnetic interactions of axions in our galactic halo, employ high-quality resonant cavities immersed in strong magnetic fields to enhance the conversion of axions into detectable microwave photons [12]. In cavity haloscopes, the axion-to-photon conversion power is given by

$$P_{a\gamma\gamma} \simeq 9.2 \times 10^{-23}\mathrm{W}\left(\frac{g_\gamma}{-0.97}\right)^2\left(\frac{\rho_a}{0.45\ \mathrm{GeV/cm^3}}\right) \times \left(\frac{\nu_a}{5.1\ \mathrm{GHz}}\right)\left(\frac{\langle \mathbf{B}_e^2\rangle}{(9.8\mathrm{T})^2}\right)\left(\frac{V_c}{1.4\mathrm{L}}\right)\left(\frac{G}{0.5}\right)\left(\frac{Q_c}{10^5}\right), \quad (1)$$

where g_γ represents the axion-photon coupling coefficient with values of -0.97 and 0.36 for the KSVZ and DFSZ models, respectively, ρ_a and $\nu_a (= m_a/2\pi)$ denote the local density and Compton frequency (mass) of the dark matter axion, $\langle \mathbf{B}_e^2 \rangle$ is the average squared external magnetic field within the cavity volume V_c, and $Q_c [= Q_l(1+\beta)]$ is the unloaded (loaded) cavity quality factor with β being the antenna coupling coefficient. The geometry factor G refers to how efficiently a resonant cavity mode couples to the

*These authors contributed equally to this work.
†Contact author: swyoun@ibs.re.kr

Published by the American Physical Society under the terms of the Creative Commons Attribution 4.0 International license. Further distribution of this work must maintain attribution to the author(s) and the published article's title, journal citation, and DOI. Funded by SCOAP³.

axion-induced electromagnetic signal:

$$G = \frac{|\int \mathbf{E}_r \cdot \mathbf{B}_e dV_c|^2}{\int \epsilon |\mathbf{E}_r|^2 dV_c \int |\mathbf{B}_e|^2 dV_c}, \quad (2)$$

where $\mathbf{E}_r$ is the electric field of the mode and ϵ is the dielectric constant inside the cavity.

Although cavity haloscopes are among the most effective methods for detecting axion dark matter, current sensitive searches are primarily limited to low-mass regions, typically within several microelectron volts, due to the practical constraints of existing experimental setups optimized for maximum detection volume. To address this, various advancements in resonator designs [13] and new detection techniques [14,15] have been explored to extend the sensitivity of axion searches into higher-mass regions. In parallel, theoretical studies, particularly within postinflationary scenarios, have constrained the plausible axion mass range based on various production mechanisms, such as misalignment and topological defects [16–24], often complemented by astrophysical observations [25,26]. They generally suggest that axions may have a mass beyond the reach of current sensitive experiments. Consequently, extending experimental searches to higher-mass regions is crucial for testing these theoretical frameworks and evaluating the viability of axions as dark matter.

Higher-order resonant modes present advantages for axion searches at high frequencies, naturally extending the search range—for instance, by factors of 2.3 and 3.6 for the TM020 and TM030 modes, respectively, compared to the fundamental TM_{010} mode—without sacrificing cavity volume while providing higher quality factors, compared to the fundamental mode. However, their practical application has been limited by small geometry factors and challenges in frequency tuning due to the complicated field variations. A recent study introduced an auxetic structure to enhance the tunability while preserving a suitable geometry factor for the TM_{020} mode [27]. Implemented in an axion search around 5.2 GHz, the mechanism enabled a 100-MHz scan with improved geometry factors, demonstrating its effectiveness for higher-order mode tuning. In this Letter, we report new results from a subsequent search achieving near-KSVZ sensitivity over an axion frequency range of 5.07–5.17 GHz, further advancing the feasibility of axion searches based on higher-order modes.

For the TM_{020} mode of a cylindrical cavity, the electric field profile comprises counteroscillating components that induce destructive energy storage under a uniform magnetic field, which can be inferred from Eq. (2), leading to a reduced geometry factor ($G = 0.15$) compared to the TM_{010} mode ($G = 0.69$). A dielectric structure placed along the cavity center suppresses one of the components, improving the quantity to ~0.5, as illustrated in Fig. 1. Additionally, Ref. [28] has demonstrated that the size of the dielectric material affects the resonant frequency. Our

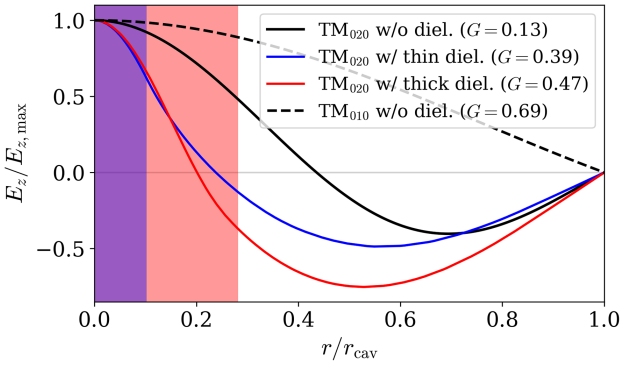

FIG. 1. Electric field profiles of the TM_{020} mode in a cylindrical cavity without (solid black line) and with (solid colored lines) a dielectric layer placed at the cavity center. The shaded regions indicate the thicknesses of the dielectric layers. The corresponding geometry factor for each configuration is also provided. For comparison, the electric field profile of the TM_{010} mode (black dashed line) is overlaid.

engineered design incorporates an array of thin dielectric rods placed at the center of the cavity. These rods are integrated with an auxetic structure that dynamically adjusts their spacing, thereby effectively altering the size of the rod assembly. The initial tuning mechanism was based on a hexagonal configuration, consisting of six individual blocks hinged to the corners of a central hexagonal block [27]. In this Letter, we adopt a modified auxetic design featuring a 3×3 square block array arranged in a regular tessellation, adopted from Ref. [29]. This design incorporates a thin dielectric rod at the central block and four thicker rods at the side blocks. Rotation of the central block adjusts the spacing between the rods at equal intervals, effectively increasing (decreasing) the thickness of the dielectric assembly when stretched (compressed). Compared to the original hexagonal configuration, the square tessellation enables more isotropic deformation while providing larger spacing intervals, thereby improving the frequency tunability, as shown in Fig. 2.

The experiment features a 12-T, ϕ96-mm superconducting solenoid and a dilution refrigerator (DR). The solenoid, operating in persistent mode, generates an average 9.8-T field within the cavity, while the DR maintains detector components below 40 mK. The cryogenic system houses the microwave cavity and a readout chain including a Josephson parametric amplifier (JPA) and two high electron mobility transistors (HEMTs). The signal is further amplified at room temperature, down-converted to an intermediate frequency, digitized, and transformed into the frequency domain for storage. A schematic of the haloscope setup is shown in Fig. 3.

The cylindrical cavity, made of 5-mm thick oxygen-free high-conductivity copper, has internal dimensions of ϕ78 mm × 300 mm, yielding a detection volume of 1.43 L. The tuning rods, fabricated from high-purity aluminum oxide ($\epsilon = 9.7, \tan\delta \sim 5 \times 10^{-6}$), have diameters of 3 mm

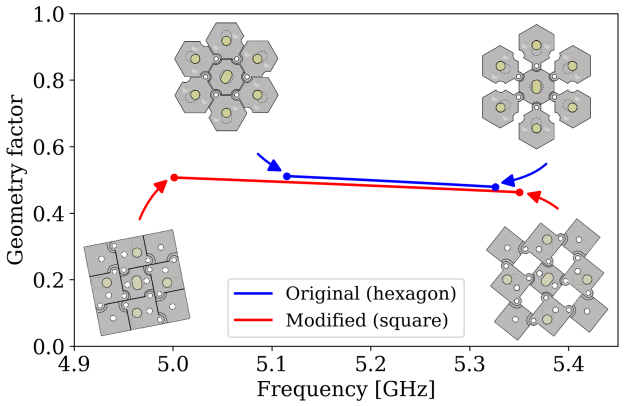

FIG. 2. Simulated geometry factors over the tunable frequency range for the original (blue) and modified (red) tuning mechanisms. The end points of each curve correspond to the fully compressed and fully extended configurations of the tuning structure.

and 7 mm for the central and side rods, respectively. The side rods feature 2-mm diameter tips on both ends for connection to a pair of tuning structures outside the cavity. To prevent friction during movement at cryogenic temperatures, the thicker section of each side rod was designed to allow a 100-μm gap from the inner surface of the end caps. Each 3×3 auxetic tuning structure, measuring $6.5 \times 6.5 \times 10$ mm^3, is constructed from aluminum, with each block thermally linked to the cavity via thin copper wires to facilitate cooling of the tuning rods. A piezoelectric actuator, coupled to the central rod via a 100:24 gear system, drives rotational tuning of the auxetic structure. Optimized through finite element simulations [30] to maintain high values of G over a practical tuning range, the rods are initially spaced 6.5 mm apart and have a travel length of 2.7 mm, enabling frequency tuning from 5.00 to 5.29 GHz. The simulation also estimates a form factor of approximately 0.5 throughout this range. The unloaded cavity quality factors were measured to be ~110 000, remaining relatively uniform over the scan.

Our flux-driven JPA, similar to the design in Ref. [31], consists of a $\lambda/4$ coplanar waveguide terminated with a dc superconducting quantum interference device. To protect it from external magnetic fields, the JPA is enclosed within a three-layer shield made of aluminum, cryoperm, and NbTi

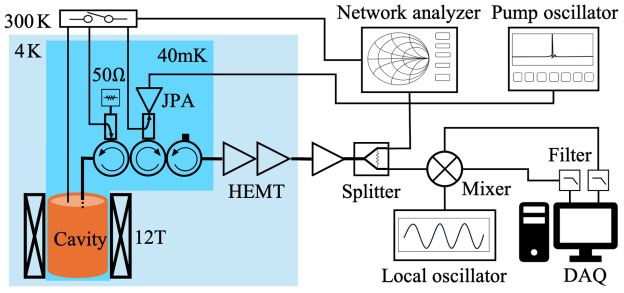

FIG. 3. Schematic of the experimental setup.

alloys. Its characteristics are dictated by a magnetic flux that modulates the nonlinear inductance of the Josephson junctions, while a microwave pump signal enables parametric amplification via three-wave mixing. Tuned by a superconducting coil, the JPA operates over the 5.00–5.32 GHz range. The JPA was operated in a phase-insensitive mode by detuning its resonance from the cavity frequency by 200 kHz.

The optimal operating conditions of the JPA were determined using the Nelder-Mead (NM) algorithm [32], a heuristic method that iteratively adjusts two parameters—flux and pump power—to find the minimum noise temperature [33]. The algorithm initializes these parameters based on prescanned resonance and gain profiles. At each iteration, a new test point is selected within the two-dimensional parameter space, and the noise temperature is estimated using the noise visibility ratio (NVR) [34,35], defined as

$$\mathrm{NVR} = \frac{P^{\mathrm{on}}}{P^{\mathrm{off}}} = \frac{G_{\mathrm{JPA}} T_{\mathrm{sys}}^{\mathrm{on}}}{T_{\mathrm{sys}}^{\mathrm{off}}}, \tag{3}$$

where the superscripts denote the pump on and off, respectively, and G_{JPA} is the JPA gain determined using a network analyzer. $T_{\mathrm{sys}}^{\mathrm{on}}$ is the system noise temperature to be measured, while $T_{\mathrm{sys}}^{\mathrm{off}}$ was estimated prior to the experiment using the Y-factor method [36], with the 50 Ω terminator in Fig. 3 serving as the noise source. The NVR-based estimation, validated by an independent Y-factor measurement, enables time-efficient *in situ* noise evaluation when integrated with the NM algorithm. The number of iterations was set to ten, which was sufficient to find the local minimum noise temperature, typically requiring one minute. The system noise was estimated to be as low as 550 mK over its tunable range with a typical gain of 20 dB.

The data acquisition (DAQ) sequence was as follows. The cavity was characterized using a network analyzer (NA): the resonant frequency and $Q_l \approx 35\,000$ from transmission measurements and $\beta \approx 2.0$ from Smith circle fitting [37]. To operate in phase-insensitive mode, the JPA resonance was detuned by approximately 200 kHz from the cavity resonance. The noise temperature was estimated using the NM algorithm by optimizing flux bias and pump power. Signals were extracted via a strongly coupled antenna and amplified sequentially by the JPA, a pair of cryogenic HEMTs, and a room-temperature HEMT. Every ten seconds, the acquired signal was down-converted to a 3-MHz intermediate frequency—a quiet region in the ambient noise spectrum—using a local oscillator and an IQ mixer. The two quadrature components were processed separately up to digitization at 20 MHz, then merged in software. The time-series data were Fourier transformed over a 1-MHz span with a resolution bandwidth of 100 Hz before stored for offline analysis. The DAQ paused every minute for a JPA sanity check, rerunning the NM algorithm if the gain deviated by more than 1 dB from the prior

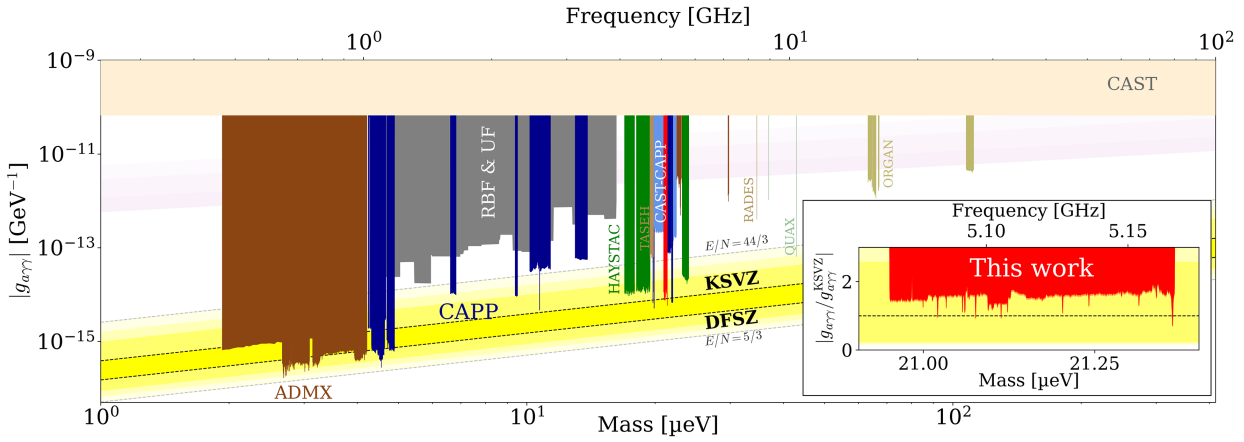

FIG. 4. Exclusion limits on axion–photon coupling as a function of axion mass from cavity haloscope searches: RBF [44,45],UF [46,47], ADMX [48–54], CAPP [55–64], HAYSTAC [65–69], TASEH [70], CAST-CAPP [71], RADES [72], QUAX [73–77], ORGAN [78–80]. The dashed black lines indicate the KSVZ and DFSZ model predictions with the yellow band representing theoretical uncertainties. The newly excluded region by this Letter is shown in red and magnified in the inset where the coupling is normalized to the KSVZ model.

measurement, which typically indicates abnormal behavior. Data were collected for 30–120 minutes per tuning step depending on the JPA performance, with a DAQ efficiency of 87.2%. The cavity was then tuned by 50 kHz, approximately one-third of its loaded bandwidth, to the next search frequency. The experiment ran from 22 August 2024 to 21 January 2025 with several interruptions due to facility maintenance, yielding a total data collection period of 152 days.

The data analysis followed the procedure outlined in [27]. For each ten-second raw spectrum, the baseline shape —affected by factors like impedance mismatch—was removed using a Savitzky-Golay (SG) filter [38], and the spectrum was normalized to this baseline. The preprocessed spectrum was rescaled to ensure consistent scaling across different frequency ranges, using the ratio $(P_{\rm sig}/\delta P_{\rm sys})^{-1}$, where $P_{\rm sig}$ is the expected signal power and $\delta P_{\rm sys}$ is the mean noise power, to reflect the frequency dependence of the cavity response. In the rescaling, the expected signal power was estimated assuming KSVZ axions with $\rho_a = 0.45$ GeV/cm^3 [39–41]. The rescaled spectra were vertically combined using inverse-variance weighting to yield a unified single spectrum spanning 5.07–5.17 GHz. For each frequency bin, power excesses in subsequent bins were weighted according to the expected axion line shape [42] and coherently combined. The axion halo model assumes virialized axions with a Maxwellian velocity distribution from the standard Halo model, yielding a quality factor of $Q_a \approx 10^6$. Repeating this over the full span produced a grand spectrum, with each bin representing its maximum-likelihood estimate.

The SG filter, applied for baseline removal, smooths the power excess and introduces correlations that influence the signal-to-noise ratio (SNR) in the final results [43]. The performance of the SG filter was evaluated through a comprehensive Monte Carlo study. The filter parameters, polynomial degree (order of the fitted polynomial) and window size (number of bins used per fit), were optimized to maximize the SNR in the presence of axion signals. Synthetic axion signals with an expected SNR $= 5.0$ were generated and overlaid onto raw baseline spectra to simulate realistic experimental conditions. For each set of filter parameters, the full analysis pipeline, including filtering, was applied to 400 datasets to ensure statistical robustness. Repeating the procedure over various parameter combinations, we identified the configuration that maximizes signal recovery as polynomial degree 4 and window size 901. This process was carried out at ten different frequencies, yielding an overall signal recovery efficiency of $\epsilon_{\rm sig} = 79.5 \pm 2.5\%$. The corresponding noise spectrum followed a normal distribution $\mathcal{N}(0.00, 0.88)$, resulting in an effective SNR of 4.59 ± 0.13.

A statistical hypothesis test was employed to evaluate the presence of an axion-induced signal in the grand spectrum. The spectrum was renormalized to unit variance to facilitate sensitivity analysis. For axions with SNR $= 5.0$, a detection threshold of 3.718 was set, corresponding to a 90% confidence level, to identify potential signal candidates. Within the scanned range, 12 candidates exceeded the threshold and were subjected to to targeted rescans at the corresponding frequencies. All excesses fell below the threshold upon rescanning, indicating them as statistical fluctuations, as supported by a quick MC study predicting approximately ten candidates for such occurrences.

Since the power excess was normalized in units of the KSVZ axion signal during rescaling, the standard deviation σ in each bin quantifies statistical fluctuations and corresponds to the inverse of the SNR for the KSVZ axion coupling strength. Accordingly, the null hypothesis was defined as an axion-induced excess corresponding to a

coupling of $\sqrt{5\sigma/\epsilon_{\rm sig}} \times g_{a\gamma\gamma}^{\rm KSVZ}$. The average σ across a total of 1 014 602 scanned frequency bins was found to be 0.449. Since no excess was observed, the null hypothesis was rejected at the 90% CL, setting an upper limit on the axion-photon coupling of $g_{a\gamma\gamma} \gtrsim 1.7 \times g_{a\gamma\gamma}^{\rm KSVZ}$ over the mass (frequency) range $20.95 - 21.37$ μeV (5.07–5.17 GHz), as shown in Fig. 4.

The final results accounted for both statistical and systematic uncertainties. The system noise temperature exhibited statistical fluctuations of approximately 30 mK throughout the experiment, as determined from measurements taken during JPA sanity checks conducted every minute at each tuning step. The statistical and fitting uncertainties in measuring the loaded quality factor, were 1.1% and 0.6%, respectively. The coupling coefficient, determined from Smith circle fitting, had a typical error of 4.2%. The uncertainty in the geometry factor was evaluated through numerical simulations considering potential misalignment of the tuning rods due to the complex tuning structure. All the rods were randomly displaced by up to 50 μm in the transverse plane and up to 100 μm along the z direction, and the geometry factor was computed for each configuration. Based on 100 three-dimensional simulations, the statistical fluctuations in the factor remained below 0.8% across the scanned frequency range.

In conclusion, we have conducted a high-sensitivity axion search near 21 μeV using the TM_{020} mode of a cylindrical cavity equipped with an innovative tuning mechanism. Our results achieved near-KSVZ sensitivity over a 100-MHz range, marking a significant advancement in axion searches at higher masses. By successfully employing a higher-order resonant mode, traditionally considered challenging for both sensitivity and tunability, this Letter demonstrates its viability for probing axions in previously unexplored mass regions. These findings not only set new constraints on the axion parameter space but also lay the groundwork for future experimental efforts targeting higher-mass axion dark matter.

Acknowledgments—This work was supported by the Institute for Basic Science (IBS-R017-D1-2024-a00 and IBS-R040-C1-2025-a00) and by JSPS KAKENHI (Grant No. JP22H04937). J. J. was partially supported by the Knut and Alice Wallenberg Foundation. Y. K. was partially supported by the Alexander von Humboldt Foundation. A. F. v. L. was supported by a JSPS Postdoctoral Fellowship. J. E. K. was partially supported by the National Academy of Science.

Data availability—The data that support the findings of this article are not publicly available upon publication because it is not technically feasible and/or the cost of preparing, depositing, and hosting the data would be prohibitive within the terms of this research project. The data are available from the authors upon reasonable request.

[1] G. Bertone and D. Hooper, Rev. Mod. Phys. **90**, 045002 (2018).
[2] R. D. Peccei and H. R. Quinn, Phys. Rev. Lett. **38**, 1440 (1977).
[3] J. E. Kim, Phys. Rev. Lett. **43**, 103 (1979).
[4] M. Shifman, A. Vainshtein, and V. Zakharov, Nucl. Phys. **B166**, 493 (1980).
[5] A. R. Zhitnitsky, Sov. J. Nucl. Phys. **31**, 260 (1980).
[6] M. Dine, W. Fischler, and M. Srednicki, Phys. Lett. **104B**, 199 (1981).
[7] J. Preskill, M. B. Wise, and F. Wilczek, Phys. Lett. **120B**, 127 (1983).
[8] L. Abbott and P. Sikivie, Phys. Lett. **120B**, 133 (1983).
[9] M. Dine and W. Fischler, Phys. Lett. **120B**, 137 (1983).
[10] C. O'Hare, cajohare/axionlimits: Axionlimits, https://cajohare.github.io/AxionLimits/ (2020).
[11] Y. K. Semertzidis and S. Youn, Sci. Adv. **8**, abm9928 (2022).
[12] P. Sikivie, Phys. Rev. Lett. **51**, 1415 (1983).
[13] J. Jeong, S. Youn, S. Bae, J. Kim, T. Seong, J. E. Kim, and Y. K. Semertzidis, Phys. Rev. Lett. **125**, 221302 (2020).
[14] A. Caldwell, G. Dvali, B. Majorovits, A. Millar, G. Raffelt, J. Redondo, O. Reimann, F. Simon, and F. Steffen (MADMAX Working Group), Phys. Rev. Lett. **118**, 091801 (2017).
[15] M. Lawson, A. J. Millar, M. Pancaldi, E. Vitagliano, and F. Wilczek, Phys. Rev. Lett. **123**, 141802 (2019).
[16] O. Wantz and E. P. S. Shellard, Phys. Rev. D **82**, 123508 (2010).
[17] M. Kawasaki, K. Saikawa, and T. Sekiguchi, Phys. Rev. D **91**, 065014 (2015).
[18] S. Borsanyi, Z. Fodor, J. Guenther, K.-H. Kampert, S. D. Katz, T. Kawanai, T. G. Kovacs, S. W. Mages, A. Pasztor, F. Pittler, J. Redondo, A. Ringwald, and K. K. Szabo, Nature (London) **539**, 69 (2016).
[19] C. Bonati, M. D'Elia, M. Mariti, G. Martinelli, M. Mesiti, F. Negro, F. Sanfilippo, and G. Villadoro, J. High Energy Phys. 03 (2016) 155.
[20] V. B. Klaer and G. D. Moore, J. Cosmol. Astropart. Phys. 11 (2017) 049.
[21] M. Dine, P. Draper, L. Stephenson-Haskins, and D. Xu, Phys. Rev. D **96**, 095001 (2017).
[22] M. Buschmann, J. W. Foster, and B. R. Safdi, Phys. Rev. Lett. **124**, 161103 (2020).
[23] M. Buschmann, J. W. Foster, A. Hook, A. Peterson, D. E. Willcox, W. Zhang, and B. R. Safdi, Nat. Commun. **13**, 1049 (2022).
[24] H. Kim, J. Park, and M. Son, J. High Energy Phys. 07 (2024) 150.
[25] L. Visinelli and P. Gondolo, Phys. Rev. D **80**, 035024 (2009).
[26] P. Gondolo and L. Visinelli, Phys. Rev. Lett. **113**, 011802 (2014).
[27] S. Bae, J. Jeong, Y. Kim, S. W. Youn, H. Park, T. Seong, S. Oh, and Y. K. Semertzidis, Phys. Rev. Lett. **133**, 211803 (2024).
[28] J. Kim, S. Youn, J. Jeong, W. Chung, O. Kwon, and Y. K. Semertzidis, J. Phys. G **47**, 035203 (2020).
[29] S. Bae, S. W. Youn, and J. Jeong, Phys. Rev. D **107**, 015012 (2023).

[30] COMSOL, Comsol multiphysics® (1998), https://www.comsol.com/comsol-multiphysics.
[31] Ç. Kutlu, A. F. Van Loo, S. V. Uchaikin, A. N. Matlashov, D. Lee, S. Oh, J. Kim, W. Chung, Y. Nakamura, and Y. K. Semertzidis, Supercond. Sci. Technol. **34**, 085013 (2021).
[32] J. A. Nelder and R. Mead, Computer J. **7**, 308 (1965).
[33] Y. Kim, J. Jeong, S. Youn, S. Bae, A. F. van Loo, Y. Nakamura, S. Uchaikin, and Y. K. Semertzidis, Electronics **13**, 2127 (2024).
[34] H. Friis, Proc. IRE **32**, 419 (1944).
[35] K. M. Sliwa, M. Hatridge, A. Narla, S. Shankar, L. Frunzio, R. J. Schoelkopf, and M. H. Devoret, Phys. Rev. X **5**, 041020 (2015).
[36] G. F. Engen, IEEE Trans. Instrum. Meas. **19**, 344 (1970).
[37] D. Kajfez and E. Hwan, IEEE Trans. Microwave Theory Tech. **32**, 666 (1984).
[38] A. Savitzky and M. J. Golay, Anal. Chem. **36**, 1627 (1964).
[39] X. Ou, A.-C. Eilers, L. Necib, and A. Frebel, Mon. Not. R. Astron. Soc. **528**, 693 (2024).
[40] N. W. Evans, C. A. J. O'Hare, and C. McCabe, Phys. Rev. D **99**, 023012 (2019).
[41] P. F. de Salas and A. Widmark, Rep. Prog. Phys. **84**, 104901 (2021).
[42] M. S. Turner, Phys. Rev. D **42**, 3572 (1990).
[43] A. K. Yi, S. Ahn, B. R. Ko, and Y. K. Semertzidis, J. High Energy Phys. 11 (2023) 115.
[44] S. DePanfilis, A. C. Melissinos, B. E. Moskowitz, J. T. Rogers, Y. K. Semertzidis, W. U. Wuensch, H. J. Halama, A. G. Prodell, W. B. Fowler, and F. A. Nezrick, Phys. Rev. Lett. **59**, 839 (1987).
[45] W. U. Wuensch, S. De Panfilis-Wuensch, Y. K. Semertzidis, J. T. Rogers, A. C. Melissinos, H. J. Halama, B. E. Moskowitz, A. G. Prodell, W. B. Fowler, and F. A. Nezrick, Phys. Rev. D **40**, 3153 (1989).
[46] C. Hagmann, P. Sikivie, N. S. Sullivan, and D. B. Tanner, Phys. Rev. D **42**, 1297 (1990).
[47] C. Hagmann, D. Kinion, W. Stoeffl, K. van Bibber, E. Daw, J. McBride, H. Peng, L. Rosenberg, H. Xin, J. Laveigne, P. Sikivie, N. Sullivan, D. Tanner, D. Moltz, F. Nezrick, M. Turner, N. Golubev, and L. Kravchuk, Nucl. Phys. B, Proc. Suppl. **51**, 209 (1996).
[48] S. J. Asztalos, G. Carosi, C. Hagmann, D. Kinion, K. van Bibber, M. Hotz, L. J. Rosenberg, G. Rybka, J. Hoskins, J. Hwang, P. Sikivie, D. B. Tanner, R. Bradley, and J. Clarke, Phys. Rev. Lett. **104**, 041301 (2010).
[49] N. Du *et al.* (ADMX Collaboration), Phys. Rev. Lett. **120**, 151301 (2018).
[50] T. Braine *et al.* (ADMX Collaboration), Phys. Rev. Lett. **124**, 101303 (2020).
[51] C. Bartram *et al.* (ADMX Collaboration), Phys. Rev. Lett. **127**, 261803 (2021).
[52] C. Boutan *et al.* (ADMX Collaboration), Phys. Rev. Lett. **121**, 261302 (2018).
[53] C. Goodman *et al.* (ADMX Collaboration), Phys. Rev. Lett. **134**, 111002 (2025).
[54] C. Bartram *et al.*, Rev. Sci. Instrum. **94**, 044703 (2023).
[55] S. Lee, S. Ahn, J. Choi, B. R. Ko, and Y. K. Semertzidis, Phys. Rev. Lett. **124**, 101802 (2020).
[56] J. Jeong, S. W. Youn, S. Bae, J. Kim, T. Seong, J. E. Kim, and Y. K. Semertzidis, Phys. Rev. Lett. **125**, 221302 (2020).
[57] O. Kwon *et al.*, Phys. Rev. Lett. **126**, 191802 (2021).
[58] Y. Lee, B. Yang, H. Yoon, M. Ahn, H. Park, B. Min, D. L. Kim, and J. Yoo, Phys. Rev. Lett. **128**, 241805 (2022).
[59] H. Yoon, M. Ahn, B. Yang, Y. Lee, D. L. Kim, H. Park, B. Min, and J. Yoo, Phys. Rev. D **106**, 092007 (2022).
[60] J. Kim, O. Kwon, Ç. Kutlu, W. Chung, A. Matlashov, S. Uchaikin, A. F. van Loo, Y. Nakamura, S. Oh, H. Byun, D. Ahn, and Y. K. Semertzidis, Phys. Rev. Lett. **130**, 091602 (2023).
[61] A. K. Yi *et al.*, Phys. Rev. Lett. **130**, 071002 (2023).
[62] B. Yang, H. Yoon, M. Ahn, Y. Lee, and J. Yoo, Phys. Rev. Lett. **131**, 081801 (2023).
[63] Y. Kim, J. Jeong, S. W. Youn, S. Bae, K. Lee, A. F. van Loo, Y. Nakamura, S. Oh, T. Seong, S. Uchaikin, J. E. Kim, and Y. K. Semertzidis, Phys. Rev. Lett. **133**, 051802 (2024).
[64] S. Ahn *et al.*, Phys. Rev. X **14**, 031023 (2024).
[65] B. M. Brubaker *et al.*, Phys. Rev. Lett. **118**, 061302 (2017).
[66] K. M. Backes *et al.*, Nature (London) **590**, 238 (2021).
[67] L. Zhong *et al.*, Phys. Rev. D **97**, 092001 (2018).
[68] M. J. Jewell *et al.* (HAYSTAC Collaboration), Phys. Rev. D **107**, 072007 (2023).
[69] X. Bai *et al.* (HAYSTAC Collaboration), Phys. Rev. Lett. **134**, 151006 (2025).
[70] H. Chang, J.-Y. Chang, Y.-C. Chang, Y.-H. Chang, Y.-H. Chang, C.-H. Chen, C.-F. Chen, K.-Y. Chen, Y.-F. Chen, W.-Y. Chiang, W.-C. Chien, H. T. Doan, W.-C. Hung, W. Kuo, S.-B. Lai, H.-W. Liu, M.-W. OuYang, Ping-I. Wu, and S.-S. Yu, Phys. Rev. Lett. **129**, 111802 (2022).
[71] C. M. Adair *et al.*, Nat. Commun. **13**, 6180 (2022).
[72] A. Álvarez Melcón *et al.*, J. High Energy Phys. 10 (2021) 075.
[73] D. Alesini *et al.*, Phys. Rev. D **99**, 101101(R) (2019).
[74] D. Alesini *et al.*, Phys. Rev. D **103**, 102004 (2021).
[75] D. Alesini *et al.*, Phys. Rev. D **106**, 052007 (2022).
[76] R. Di Vora *et al.* (QUAX Collaboration), Phys. Rev. D **108**, 062005 (2023).
[77] A. Rettaroli *et al.* (QUAX Collaboration), Phys. Rev. D **110**, 022008 (2024).
[78] B. T. McAllister, G. Flower, E. N. Ivanov, M. Goryachev, J. Bourhill, and M. E. Tobar, Phys. Dark Universe **18**, 67 (2017).
[79] A. Quiskamp, B. T. McAllister, P. Altin, E. N. Ivanov, M. Goryachev, and M. E. Tobar, Sci. Adv. **8**, eabq3765 (2022).
[80] A. Quiskamp, B. T. McAllister, P. Altin, E. N. Ivanov, M. Goryachev, and M. E. Tobar, Phys. Rev. Lett. **132**, 031601 (2024).